Cross-Correlation Analysis of Inner-Leaflet-Anchored Green Fluorescent Protein Co-Redistributed with IgE Receptors and Outer Leaflet Lipid Raft Components

Paul S. Pyenta, David Holowka, and Barbara Baird
Department of Chemistry and Chemical Biology, Baker Laboratory, Cornell University, Ithaca, New York 14853 USA

ABSTRACT To investigate the structural basis for membrane interactions that occur between Lyn tyrosine kinase and IgE-FcεRI or other components of lipid rafts, we prepared a green fluorescent protein analog of Lyn (PM-EGFP) and used cross-correlation analysis to quantify co-redistributions of aggregates that occur after IgE-FcεRI is cross-linked on the cell surface. PM-EGFP, which contains minimally the palmitoylation and myristoylation sites on Lyn, was compared with another inner leaflet probe, EGFP-GG, which contains a prenylation site and a polybasic sequence similar to K-ras. Confocal fluorescence microscopy was used to examine co-redistributions of these inner leaflet components with IgE-FcεRI and outer leaflet raft components, ganglioside GD_{1b} and glycosylphosphotidylinositol-linked Thy-1, under conditions where the latter were cross-linked externally to form large patches at the cell surface. The cross-correlation analysis was developed and characterized with simulations representing cell surface distributions, and parameters from the cross-correlation curves, ρ_o (peak height) and A (peak area), were shown to be reliable measures of the extent of co-redistributed aggregates and their size. Cross-correlation analysis was then applied to quantify co-redistributions of the fluorescently labeled inner and outer leaflet components on RBL-2H3 cells. As visually observed and parameterized in this manner, PM-EGFP was found to co-redistribute with lipid rafts significantly more than EGFP-GG or an endogenous prenylated protein, Cdc42. These quantitative results are consistent with previous analyses of Lyn co-redistributions and support the hypothesis that the functionally important interaction of Lyn with cross-linked IgE- FcεRI is due to their mutual co-association with lipid rafts.

INTRODUCTION

Mast cells and basophils are stimulated to degranulate when multivalent antigen cross-links IgE bound to their transmembrane, high-affinity receptors, FcεRI. The first recognized biochemical event of the cytoplasmic signal transduction cascade involves tyrosine phosphorylation of β and γ subunits of FcεRI by Lyn, a member of the Src family of tyrosine kinases (Kinet, 1999). Although a detailed understanding of the interactions leading to phosphorylation has not yet been achieved, accumulating evidence indicates that the plasma membrane structure plays a critical role in the process. Membrane domains, sometimes called lipid rafts, are proposed to coalesce around the aggregated receptors, and these serve as foci for FcεRI-Lyn coupling and initiation of signal transduction (Sheets et al., 1999b). Similar models have also been proposed for T-cell receptors (Montixi et al., 1998; Xavier and Seed, 1999; James et al., 2000). Previously published results show that isolated rafts are enriched in phospholipids with saturated fatty acid chains, glycosphingolipids, cholesterol, and glycosylphosphatidylinositol (GPI)-anchored proteins (Brown and London, 1998b; Fridriksson et al., 1999). Src kinases, including Lyn, that are anchored to the inner leaflet by saturated palmitate and myristate acyl chains also associate with these membrane rafts (Field et al., 1995; Webb et al., 2000).

Although detailed physical properties of membrane rafts have not been elucidated (Brown and London, 1998a), selective partitioning into them by Lyn and other components may be based on non-ideal mixing or lipid phase separation. Isolated rafts have been shown to have the properties of liquid ordered phases: fluid, but with gel-like ordering due to the presence of cholesterol (Schroeder et al., 1998; Ge et al., 1999). The nature of rafts on the cell membrane before and after IgE- FcεRI aggregation and the manner of their participation in receptor-mediated signaling are issues of ongoing investigation (Baird et al., 1999).

Direct evidence for the association of FcεRI and Lyn within rafts upon receptor cross-linking is still limited. Co-association within isolated, detergent-resistant membrane fractions that correlate with rafts (Field et al., 1995; Brown and London, 1997) has been demonstrated using sucrose density gradients of Triton-X-100-lysed cells. Anti-Lyn labeling of fixed and permeabilized cells showed that co-redistribution of Lyn with cross-linked FcεRI is regulated by stimulated actin polymerization (Holowka et al., 2000) and prevented by reducing cellular cholesterol with methyl-β-cyclodextrin (Sheets et al., 1999a). However, coupling between inner leaflet components such as Lyn and outer leaflet raft components has not been systematically investigated in intact cells. For this purpose, we utilized a green fluorescent protein (GFP) construct as an endogenous Lyn analog.

As now well documented and widely used, GFP (Tsien, 1998) allows fluorescent tagging of intracellular proteins.

Received for publication 19 July 2000 and in final form 10 February 2001.

Address reprint requests to Dr. Barbara A. Baird, Departments of Chemistry and Cell Biology, Baker Laboratory, Cornell University, Ithaca, NY 14853-1301. Tel.: 607-255-4095; Fax: 607-255-4137; E-mail: bab13@cornell.edu.

0006-3495/01/05/2120/13 $2.00

The GFP construct PM-EGFP described in this study contains the N-terminal 20 amino acids of Lyn that anchor it to the membrane inner leaflet because of included modification sites for myristate and palmitate (van't Hof and Resh, 1997). We prepared a second GFP construct, EGFP-GG, which anchors to the inner leaflet by polyunsaturated geranylgeranylate and a polybasic sequence. We compared the membrane distribution of PM-EGFP and EGFP-GG with respect to IgE-FcϵRI and to characteristic raft components, α-galactosyl ganglioside GD_{1b} and GPI-linked protein Thy-1. We also compared Cdc42, an endogenous cytoplasmic GTP-binding protein of the Rho family that has a geranylgeranyl membrane anchor.

We examined membrane distributions with fluorescence confocal microscopy, and equatorial profiles were quantified with cross-correlation analysis. This quantitative approach has been used previously to compare co-localization of FcϵRI and other cellular components (Stauffer and Meyer, 1997; Sheets et al., 1999a), but its application has not yet been well characterized or evaluated. As described in this paper, we examined realistic simulations and used these to interpret cross-correlation analysis of the fluorescently labeled species on RBL-2H3 cells. We demonstrate the general utility of cross-correlation Pearson coefficient, ρ_0, and peak area, A, as single-parameter representations of cross-correlation that can be used interdependently to obtain a concise description of the co-redistributing species. This computational approach can be powerfully applied to quantify confocal microscopy investigations of membrane-bound species distributions.

MATERIALS AND METHODS

EGFP constructs

PM-EGFP was constructed by inserting a base pair sequence into the multiple cloning site (MCS) of the pEGFP-N1 vector (Clontech Laboratories, Palo Alto, CA). The insert uses the N-terminal sequence for Lyn that codes for the myristoyl (M) and palmitoyl (P) fatty acylation sites (Rider et al., 1994) and includes the 60-base-pair sequence 5′-GCC CCG AAA CTT CCA CCG CGA GCG AGA AAT **ATG** GGA TGT ATT AAA TCA AAA AGG AAA GAC-3′ centered about the ATG start codon (in bold), flanked by sticky end restriction sites *Nhe*I and *Bgl*II (not shown) and adenine spacers before *Bgl*II to maintain the proper expression reading frame. The translated protein is EGFP with the N-terminus and acyl anchors of Lyn:

N′-mGCIKSKRKDNLNDDGVCMKT-[EGFP]-C′
  | |
  MP

EGFP-GG was constructed by inserting a base pair sequence into the multiple cloning site of the pEGFP-C1 (Clontech). The insert was modeled after the C-terminal sequence for K-*ras*, which codes for the fatty acylation site and polybasic region (James et al., 1995) and includes the 60-base-pair sequence 5′-GAT GGT AAA AAG AAG AAA AAG AAG TCA AAG ACA AAG TGT CAG CTG CTT **TAA TAG**-3′ and two stop codons TAA and TAG (in bold) and is flanked by sticky end restriction sites *Bgl*II and *Pst*I (not shown). The base pairs encoding the expressed CAAX box for K-*ras* (CVIM) were altered to express the CAAX box from rap1B (CQLL), resulting in geranylgeranylation (G; instead of farnesylation) of the expressed protein (Glomset and Farnsworth, 1994).

N′-[EGFP]-DGKKKKKKSKTKCQLL-C′
  ←——————→ |
  polybasic G

Both sense and anti-sense oligonucleotide sequences for PM-EGFP and EGFP-GG were synthesized, purified, and 5′ phosphorylated in the DNA Synthesis Facility (Cornell New York State Center for Advanced Technology, Ithaca, NY).

EGFP vectors were digested with restriction enzymes (New England Biolabs, Beverly, MA), separated by 1% agarose gel electrophoresis, and extracted from the gel with GeneClean Kit (Bio101, Carlsbad, CA). Complementary insert sequences were annealed and ligated to the digested vectors with T4 DNA ligase (New England Biolabs). The completed vectors were transformed into DH5α-$CaCl_2$ competent *Escherichia coli* cells that had been heat shocked at 42°C for 1 min by gently shaking at 37°C for 2 h. Cell colonies were grown on agar plates with 30 μg/ml kanamycin selection agent.

Single colonies were grown in Luria Broth medium with 30 μg/ml kanamycin overnight at 37°C, and the vector was isolated with a MiniPrep kit (Qiagen, Valencia, CA). Positive colonies were identified by restriction mapping: *Nco*I for PM-EGFP and *Bgl*II and *Mlu*I for EGFP-GG (New England Biolabs). Selected colonies were grown over several days in Luria Broth medium with 30 μg/ml kanamycin, and the vector was purified with a MidiPrep kit (Qiagen).

UV-visible spectroscopy was used to measure vector concentration and purity; the 260/280 absorption ratio was 1.7 and 1.6 for PM-EGFP and EGFP-GG vectors, respectively. Sequences of the purified vectors were confirmed by the DNA Synthesis Facility (Cornell), using primers from Clontech.

Cell lines

RBL-2H3 cells were maintained in monolayer cultures and harvested with trypsin-EDTA (Life Technologies, Rockville, MD) 3–5 days after passage, as described previously (Pierini et al., 1996). PM-EGFP and EGFP-GG constructs were transfected into RBL cells using lipofectamine reagent (Life Technologies), and transfected cells were selected with 2 g/L geneticin G418 (Life Technologies). Stable cell lines expressing either PM-EGFP or EGFP-GG were found to be similar to wild-type RBL-2H3 cells in their degranulation response to antigen as measured by β-hexosaminidase release (data not shown; Pierini et al., 1996). Transfected cells were cultured in medium without phenol red and with 500 mg/L geneticin G418; we found that cells maintained at sub-confluent densities expressed higher levels of EGFP.

Treatments with antibodies

Mouse monoclonal anti-2,4-dinitrophenyl IgE was purified as previously described (Subramanian et al., 1996) and modified with Cy3 (Amersham Pharmacia Biotech, Piscataway, NJ) according to manufacturer's instructions. The labeled IgE was shown to be monomeric by 1) characteristic migration in HPLC gel permeation chromatography and 2) capacity to trigger degranulation in RBL-2H3 cells only after addition of antigen. UV-visible absorption spectroscopy analysis showed a dye/IgE stoichiometry of 6 to 9. Monoclonal antibodies AA4 specific for α-galactosyl ganglioside GD_{1b} (a gift from Dr. Reuben Siraganian, National Institutes of Health, Bethesda, MD) (Guo et al., 1989) and OX7 specific for GPI-linked protein Thy-1 (BD Pharmingen, San Diego, CA) were labeled with Cy3 under the same conditions and with similar stoichiometries.

Stably transfected cells expressing the PM-EGFP or EGFP-GG constructs were resuspended at 5×10^6 cells/ml in buffered saline solution (BSS: 135 mM NaCl, 5.0 mM KCl, 1.8 mM $CaCl_2$, 1.0 mM $MgCl_2$, 5.6 mM glucose, 20 mM HEPES, pH 7.4) containing 5 mg/ml bovine serum albumin (BSA). They were then subjected to the following conditions for experimental comparison (Table 1). For condition 1, primary monoclonal antibodies Cy3-IgE, Cy3-AA4, and Cy3-OX7 were added to cell aliquots at 5 μg/ml for 30 min at 22°C (Cy3-AA4 and Cy3-OX7) or 37°C (Cy3-IgE). Unlabeled IgE (5 μg/ml) was co-added to the Cy3-AA4 and Cy3-OX7 samples to block binding of the IgG antibodies via their Fc segments to FcϵRI. After the incubation period, cells were sedimented, rinsed, and resuspended three times with cold (4°C) BSS/BSA. Cells labeled under condition 1 were then maintained at 4°C, and their bound Cy3-antibodies were (condition 2b) or were not (condition 2a) externally cross-linked on the cell surface as follows. To Cy3-IgE samples, multivalent antigen 2,4-dinitrophenyl-BSA was added at 2 μg/ml or anti-IgE antibody was added at 10 μg/ml. To Cy3-AA4 and Cy3-OX7 samples, anti-IgG (γ chain specific) was added at 10 μg/ml. All samples continued incubation for 4 to 6 h at 4°C. Halfway through this incubation, the cell buffer was exchanged to replenish the supply of glucose.

Confocal microscopy

At each of two points during the treatments described above (Table 1) cells were fixed for confocal imaging: 1) immediately after washing the cells labeled with primary monoclonal antibody (condition 1) and 2) after the subsequent 4- to 6-h incubation at 4°C with (condition 2b) or without (condition 2a) secondary reagent. For each condition, cells were warmed to 37°C for 10 min and then fixed by sedimentation and resuspension in phosphate-buffered saline (PBS: 150 mM NaCl, 10 mM sodium phosphate, 1 mM EDTA, pH 7.4) containing 4% formaldehyde for 15 min at 22°C. Following re-sedimentation, fixed cells were resuspended in PBS with 5 mg/ml BSA and stored at 4°C. Staining of Cdc42 in RBL-2H3 cells treated as in condition 2b was carried out by fixation in 3.7% formaldehyde and permeabilization with 0.1% Triton X-100, followed by addition of anti-Cdc42 and Cy3-anti-rabbit γ chain (Holowka et al., 2000).

Microscopy was carried out in the Imaging Facility (Cornell New York State Center for Advanced Technology, Ithaca, NY). We used a Zeiss Axiovert 10 inverted epifluorescence microscope attached to an MRC-600 confocal system (Bio-Rad Laboratories, Hercules, CA), including a Kr/Ar mixed-gas ion laser (Ion Laser Technology, Salt Lake City, UT), scanning head, and computer with COMOS software. Using a standard microscope slide and number 1 coverslip, 10-μl samples were examined with an oil immersion 100×, 1.4 NA objective. Confocal slits were set at 1/3, and simultaneous two-color photomultiplier tube detection in direct mode was used for image acquisition as previously described (Pierini et al., 1996).

Cross-correlation analysis

This mathematical method effectively searches equatorial intensity traces for similar, correlative patterns. The correlation function is closely related to the simpler convolution function:

$$f * g(x) = \lim_{T\to\infty} \int_{-T}^{+T} f(t) \times g(x - t)dt \tag{1}$$

If displacements from the function averages are incorporated into Eq. 1, the result is the cross-covariance:

$$f \circ g(x) = \lim_{T\to\infty} \int_{-T}^{+T} (f(t) - \bar{f}) \times (g(x - t) - \bar{g})dt \tag{2}$$

For N data points covering the length of the equatorial fluorescence trace, the discrete (non-normalized) form of the cross-covariance (Eq. 2) is:

$$(f \circ g)_j = \frac{1}{N} \sum_i (f_i - \bar{f}) \times (g_{i+j} - \bar{g}) \tag{3}$$

Dividing by the standard deviations of each function yields the normalized cross-correlation function:

$$\rho_j = \frac{\frac{1}{N} \sum_i (f_i - \bar{f}) \times (g_{i+j} - \bar{g})}{\left[\frac{1}{N} \sum_i (f_i - \bar{f})^2\right]^{1/2} \times \left[\frac{1}{N} \sum_i (g_i - \bar{g})^2\right]^{1/2}} = \frac{(f \circ g)_j}{\sigma_f \sigma_g} \tag{4}$$

The application of cross-correlation analysis to confocal images is a multi-step process. Digitized images were converted from BioRad format to TIFF files using the software Confocal Assistant version 4.02 (T. C. Brelje, University of Minnesota). Quantitative equatorial profiles from dually labeled, representative cells were then acquired using the free-hand selection tool of Scion Image (Scion Corp., Frederick, MD) to trace the cell circumference. The profile data files were imported into Sigma Plot version 5.0 (SPSS, Chicago, IL), for which several transforms were written. First, because there were 1.4 pixels per length of microscope resolution, the pixels were averaged pair-wise to avoid correlation of systematic instrument noise. Second, each profile pair was cross-correlated according to Eq. 4. Third, a series of transforms averaged the individual cross-correlation curves together. The resulting average was plotted on a micrometer scale, as illustrated in Fig. 6.

A reduced expression for the normalized cross-correlation function is the Pearson correlation coefficient, ρ_o, which results from setting $j = 0$ in Eq. 4 (Barlow, 1989) and corresponds to the height of the central peak of the cross-correlation curve (for example, Fig. 2). The ρ_o value corresponds to the cross-correlation at perfect alignment of paired image profiles; it does not contain any information about aggregate size.

The integrated area under the cross-correlation curve, A, includes peak height and width and thereby contains information about the degree of

TABLE 1 Experimental comparisons

Inner-leaflet component	Membrane anchorage	Cross-correlation with raft components	Conditions
PM-EGFP	Palmitate myristate (Lyn analog)	IgE-FcεRI (IgE receptor)GD_{1b} (α-galactosyl ganglioside)	1) 22°C, 30 min, with fluorescent primary antibody
EGFP-GG	Geranylgeranylate polybasic residues	Thy-1 (GPI-linked protein)	2a) Additional 4–6 h at 4°C 2b) Additional 4–6 h at 4°C, with secondary antibody or multivalent antigen
Cdc42	Geranylgeranylate	IgE-FcεRI (IgE receptor)	2b) Additional 4–6 h at 4°C, with secondary antibody or multivalent antigen

correlation and the size of the correlated aggregates. Because Eq. 4 is normalized, A values are directly comparable to one another. The A value is simply determined after fitting the computed average cross-correlation curve; we found that an exponential decay, reflective about the y axis, provides a good fit of the cross-correlation curve using a standard nonlinear least-squares procedure. Thus, to calculate A, we integrate the fitting function over all of x space:

$$A = \int_{-\infty}^{+\infty} h \times \exp\left[\frac{-|x - x_{\max}|}{w}\right] dx = 2hw, \qquad (5)$$

where h is the pre-exponential peak height, w is the peak half-width corresponding to $h[\exp(-1)]$, and $x_{\max}$ allows a small deviation from zero at which the observed peak maximum is observed. These least-squares fits were weighted as $wt = \exp[-|x - x_{\max}|]$; the tails of the correlation curve are not important and contribute vanishingly to the fit criteria. The fits of the averaged curves (Fig. 6) yield parameters h and w and thereby A (Eq. 5; Fig. 9). Note that the parameter $x_{\max}$ does not affect the value of A.

THEORETICAL RESULTS

To investigate the general features of cross-correlation analysis of two different components that may co-localize on a cell surface, we simulated representative series of equatorial intensity profiles based on those observed for RBL cells (Fig. 1). We used two baseline models: 1) flat, Fig. 1 *a*, and 2) rolling, Fig. 1 *b*. Upon these baselines we built two levels of aggregation: 1) large, Fig. 1 (solid line), and 2) small, Fig. 1 (dashed line). The rolling baseline model, although adding complexity to the analysis, is more representative of true cell membrane profiles. We designed the small aggregates to overlap partially with the large aggregates to investigate partial co-aggregation (Fig. 1, *a* and *b*). Noise was added randomly, with a normal distribution, to the profile intensity curves in Fig. 1, *a* and *b*. Relatively small and large amounts of noise are illustrated in Fig. 1, *c* and *d*, respectively. An additional profile was designed to be converse to the large profile (Fig. 1 *e*).

To simulate co-redistribution of membrane species, two new profiles were generated by adding random noise separately to one original profile of a given type (e.g., flat, large), and these were subjected to cross-correlation analysis. Fig. 2 shows selected correlative pairs. Noise was added incrementally for each case. The flat with flat case (Fig. 2 *a*) shows no correlation and serves as a negative standard. The rolling baseline positively cross-correlates with itself (Fig. 2 *b*), producing a large, wide peak not observed with the flat baseline. However, the peak depends on the intensity of the rolling baseline relative to the amount of noise; the correlation quickly diminishes with increasing noise. The large with large (Fig. 2 *c*) and small with small (Fig. 2 *d*) cases both show strong, positive correlations as expected. Cross-correlations of these two profiles with a flat baseline (not shown) are indistinguishable from those with a rolling baseline. These comparisons show that the width of the cross-correlation peak is related to the size of correlated aggregates, and this can be quantified with Eq 5. The negative values adjacent to the main peaks in Fig. 2 are due to anti-correlation, i.e., displacements equal in size to the average co-aggregated patch. In general, increasing noise diminishes the cross-correlation magnitude.

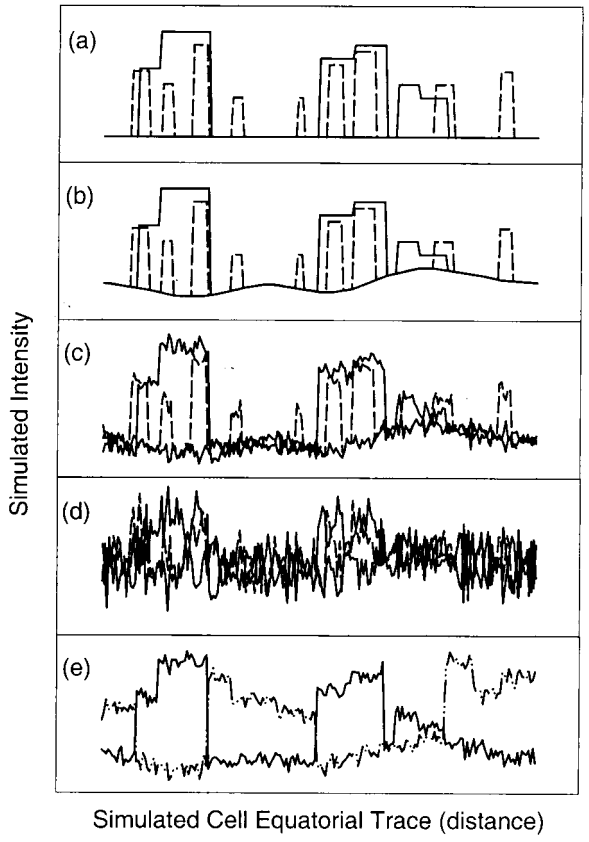

FIGURE 1 Simulated equatorial intensity profiles to model fluorescently labeled cells. Large (——) and small (– – –) aggregates were built upon either (*a*) a flat background, or (*b*) a rolling background. Some small aggregates were set to overlap the large ones. Randomly generated noise was added to the profiles in (*b*) in lesser (*c*) and greater (*d*) magnitude. An anti-large profile (*e*), including noise, was generated conversely to the large profile; i.e., aggregates were placed between the previous large ones with no overlap.

To investigate non- or partially co-aggregated species, we applied the cross-correlation analysis to mismatched profiles, as shown in Fig. 3. The flat baseline does not correlate with large aggregates (Fig. 3 *a*) or small (not shown). In contrast, overlapping large and small aggregates yield a positive cross-correlation for both flat (not shown) and rolling baselines (Fig. 3 *d*). The cross-correlation with the baseline only is not centered for either large (Fig. 3 *b*) or small (Fig. 3 *c*) aggregates. Positive cross-correlation occurs at nonzero displacements for individual comparisons, but these off-center peaks cancel out when several cell profiles are averaged (see below). The off-center peaks in Fig. 3 illustrate the possibly sizable magnitude of randomly occurring cross-correlations in any given pair.

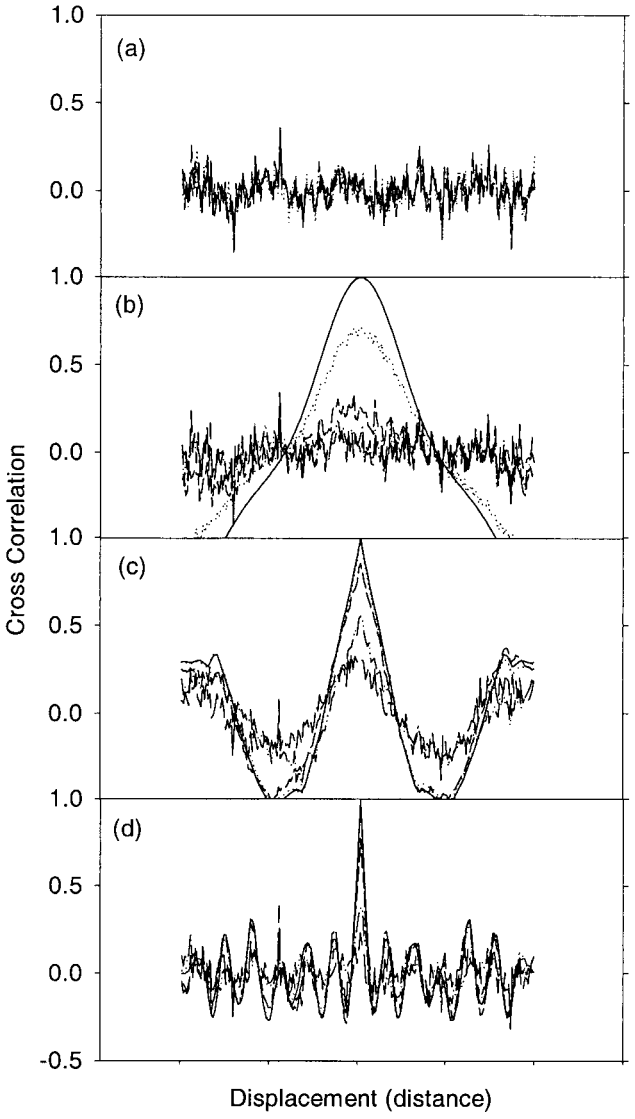

FIGURE 2 Cross-correlations of simulated equatorial intensity profiles. To generate each cross-correlation, noise was added independently to a given simulated profile to yield two traces with different, random noise fluctuations. These were then cross-correlated with Eq. 4. Within each panel, noise was added in increasing magnitude (least noise ——; most noise, – – –), and the resulting cross-correlations are represented by the line traces. Correlated simulated profile pairs presented are: *a*, Flat with flat; *b*, rolling with rolling; *c*, large with large aggregates (built upon rolling background); and *d*, small with small aggregates (built upon rolling background). Note that, because the standard deviation of a perfectly flat, noiseless line is zero, Eq. 4 is undefined, and the corresponding cross-correlation is not present in (*a*). Note that cross correlations of intensity profiles built upon a flat background were similar to (*c*) and (*d*). Displacement is in consistent, arbitrary units representing distance.

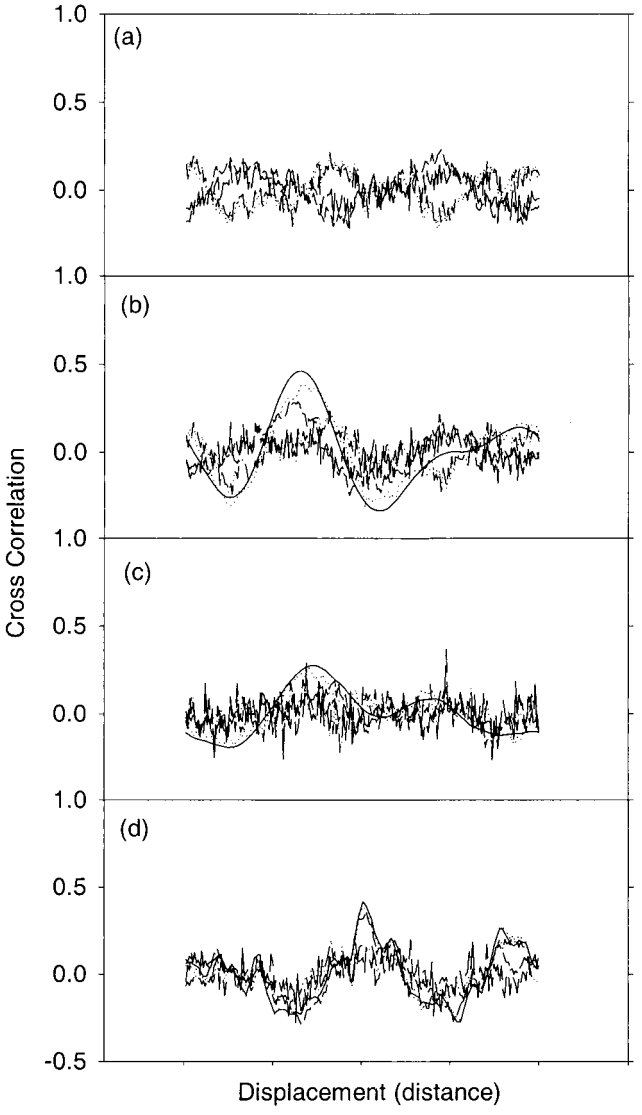

FIGURE 3 Cross-correlations (Eq. 4) of mismatched pairs of simulated equatorial intensity profiles. Within each panel, noise was added to the original profiles in increasing magnitude (least noise ——; most noise, – – –). Correlated simulated profile pairs presented are: *a*, Flat with large aggregates; *b*, rolling base with large aggregates; *c*, rolling base with small aggregates; and *d*, large with partially overlapping small aggregates (see Fig. 1 *b*). Note that cross correlations of intensity profiles built upon a flat background analogous to (*d*) were similar, and analogous to (*c*) differed only in the absence of off-center minor peaks. Displacement is in consistent, arbitrary units representing distance.

The anti-large profile, when compared with the large profile (Fig. 1 *e*), predictably results in a strong anti-correlation with a negative central peak (Fig. 4 *a*). Analogous to the results with positively correlated profiles, oppositely correlated regions exist adjacent to the main peak, and noise diminishes the anti-correlation.

As described above, the off-center peaks that result from random cross-correlations at nonzero displacements can be of substantial magnitude for any matched pair of cells. However, they average to zero over many cell pair analyses. Fig. 4 *b* shows the results of averaging over simulated cell pairs, each pair with a different set of randomly distributed large aggregates and added noise. The central peak remains after averaging because it represents a physically true cross-

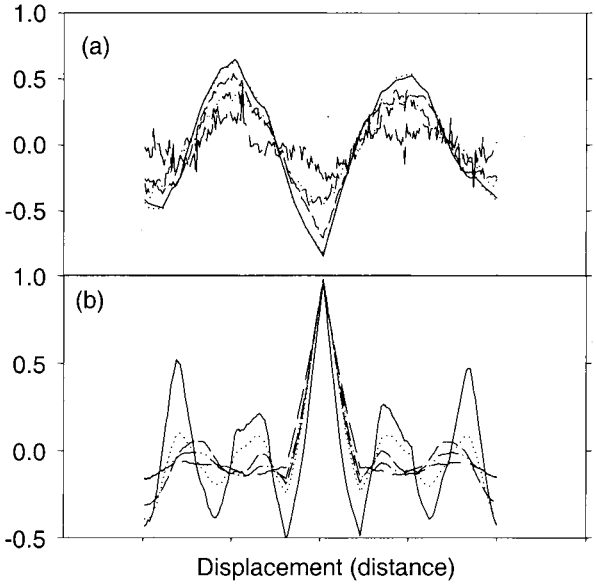

FIGURE 4 Effects on cross-correlation curves. (*a*) Strong anticorrelation results from application of Eq. 4 to simulated large and antilarge aggregate profiles (see Fig. 1 *e*); increasing noise lessens the effect (least noise ——; most noise – – –). (*b*) Averaging effects were assessed by generating several different profiles containing large aggregate patches (similar to Figure 1 *b*), and pairs of these with additional random noise were cross correlated as in Fig. 2 *c*. Averaging over the resulting correlation curves retains the main, central, whereas off-center peaks disappear with an increasing number of individual profiles. The number of correlation curves included in each average is 1 (——), 3, 6, 10, and 40 (– – –).

correlation; the off-center peaks quickly vanish with increasing number of different pairs that are averaged.

In summary, these cross-correlation analyses of simulated cell profiles demonstrate that 1) co-aggregated species produce strong positive correlations represented by peak height and peak widths provide a measure of average aggregate size, 2) membrane morphology alone can also produce positive correlations, but this is diminished by noise, 3) off-center peaks can arise from any matched pair, but these are flattened with averaging, and 4) averaged cross-correlation curves, rather than those coming from individual cell pairs, are most useful because they minimize spurious correlations.

Table 2 summarizes for various possibilities of cross-correlation peak maximum (minimum) values as represented by ρ_o (Eq. 4). Included are both the theoretical limits for perfect matches and mismatches and the ranges typically observed for comparisons on real RBL-2H3 cells. Although membrane morphology alone can yield a sizeable cross-correlation value, this is shifted down from the range of values observed for co-aggregated species.

EXPERIMENTAL RESULTS

Confocal images of dually labeled RBL cells

We showed previously that co-redistribution of Lyn with cross-linked IgE-FcϵRI correlates with their mutual interactions with lipid rafts and with initiation of transmembrane signaling (Field et al., 1997; Sheets et al., 1999b). To investigate the essential structural requirements for these interactions in intact cells, we prepared an EGFP-Lyn construct, PM-EGFP, that contains the minimal Lyn sequence necessary to cause lipid raft association via dual myristoyl and palmitoyl acylation as previously established for related Src-family kinases Fyn and Lck (Shenoy-Scaria et al., 1993; van't Hof and Resh, 1997). This was compared with another EGFP construct that was targeted to the membrane by virtue of its polybasic residues and geranylgeranyl modification site (EGFP-GG). The lateral membrane distributions of these EGFP constructs were compared with distributions of IgE-FcϵRI (transmembrane) and the outer leaflet raft components GPI-linked protein Thy-1 and ganglioside α-galactosyl-GD_{1b}. Fig. 5 shows confocal micrographs of these different samples with representative image pairs of PM-EGFP (Fig. 5 *A*) or EGFP-GG (Fig. 5 *B*) on the left side and one of the other Cy3-labeled components on the right side. RBL-2H3 cells with stably expressed EGFP constructs were labeled with Cy3-IgE, Cy3-Ox7, or Cy3-AA4 (Table 1, condition 1) before washing and treating for the initial micrographs (top row).

After this initial labeling with the Cy3-conjugated monoclonal antibodies, the micrographs show equatorial stains, indicating these labels to be on the surface with very little if any label inside the cell (Fig. 5 *A* and *B*, *top row*, right cell of image pairs). Equatorial staining confirms efficient targeting of PM-EGFP and EGFP-GG to the plasma membrane (top row, left cell of image pair). Quantitative line scans across the middle of more than 20 of these images showed the ratio of plasma membrane/cytosolic EGFP intensities to be greater than 4 for both PM-EGFP and EGFP-GG. Identical analysis with images of cells labeled only with Cy3-IgE, where the intracellular intensity comes from background autofluorescence and out-of-plane Cy3 fluorescence, shows a membrane/cytosol ratio of ~8. To test which leaflet of the plasma membrane contains the EGFP constructs, we used anti-GFP (polyclonal IgG) followed by Cy3-conjugated anti-IgG to label cells expressing the EGFP constructs after fixation with 4% formaldehyde with or without permeabilization with 0.1% Triton X-100. Confocal

TABLE 2 Summary of theoretical and experimentally observed cross-correlation values

Condition	Cross-correlation ρ_o
Theoretical limits:	
Maximum positive correlation	+1
Minimum anti-correlation	−1
No correlation	0
Observed ranges with RBL cells:	
No correlation on cell surface	$-0.2 \cdots +0.2$
Membrane topology/uniform distribution	$0 \cdots +0.6$
Co-aggregated species	$+0.4 \cdots +1$

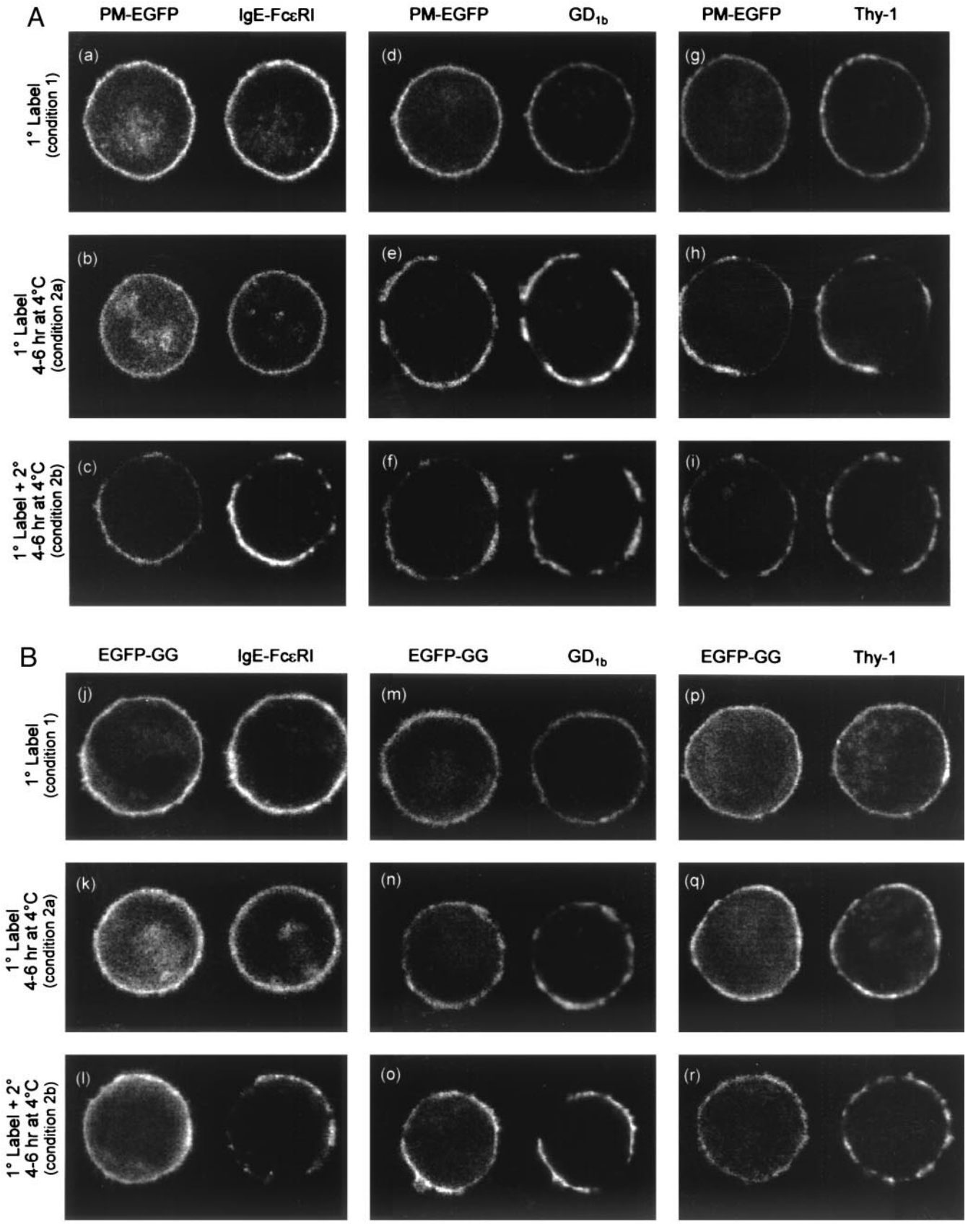
A
PM-EGFP
IgE-FcεRI
PM-EGFP
GD1b
PM-EGFP
Thy-1
1° Label (condition 1)
1° Label 4-6 hr at 4°C (condition 2a)
1° Label + 2° 4-6 hr at 4°C (condition 2b)
(a)
(b)
(c)
(d)
(e)
(f)
(g)
(h)
(i)
B
EGFP-GG
IgE-FcεRI
EGFP-GG
GD1b
EGFP-GG
Thy-1
1° Label (condition 1)
1° Label 4-6 hr at 4°C (condition 2a)
1° Label + 2° 4-6 hr at 4°C (condition 2b)
(j)
(k)
(l)
(m)
(n)
(o)
(p)
(q)
(r)

FIGURE 5

images compared for these cells confirmed PM-EGFP and EGFP-GG localization on the membrane inner leaflet (data not shown).

Under condition 1 (Table 1; Fig. 5 *A* and *B*, *top row*) there are some small differences in the homogeneity of the equatorial stain. IgE-FcϵRI generally appears uniform whereas Thy-1 and GD_{1b} exhibit limited patching in some cells, possibly resulting in the latter cases from cross-linking by the bivalent monoclonal antibodies used for their initial Cy3 labeling. In all of these image pairs, both EGFP constructs (Fig. 5 *A* and *B*, *top row*, left cell) appear mostly homogeneously distributed on the membrane.

Fig. 5 *A* and *B*, *middle* and *bottom rows*, represent confocal images of cells from the same samples after a subsequent 4- 6-h incubation at 4°C, without (Table 1, condition 2a) or with (Table 1, condition 2b) secondary cross-linking, respectively. This incubation was carried out in the cold to prevent internalization and morphological changes that depend on stimulated actin polymerization and result in the time-dependent reversal of FcϵRI-Lyn interactions (Holowka et al., 2000). The prolonged incubation time is necessary to allow large-scale patching of cross-linked species. After the cold incubation alone (condition 2a), IgE-FcϵRI remains uniformly distributed (Fig. 5 *A b* and Fig. 5 *B k*) whereas both GD_{1b} and Thy-1 form large aggregates (Fig. 5 *A*, *e* and *h*, and Fig. 5 *B*, *n* and *q*, respectively), consistent with the coalescence of membrane domains. In the presence of a secondary cross-linking agent (condition 2b), all exogenously labeled species form large aggregates (Fig. 5, *A* and *B*, *bottom row*, right side of image pairs). As shown in the left half of these image pairs, PM-EGFP clearly co-redistributes with cross-linked IgE-FcϵRI, GD_{1b}, and Thy-1 (Fig. 5 *A*, *c*, *f*, and *i*); EGFP-GG also co-redistributes (Fig. 5 *B*, *l*, *o*, and *r*), but visually to a lesser extent than PM-EGFP.

Cross-correlation analysis of paired images

Co-redistributions of membrane species, visualized as matched pairs in Fig. 5, were quantified by cross-correlation analysis (Eq. 4). As depicted in Figs. 6 *A* and 6 *B*, respectively, cross-correlation curves of PM-EGFP and EGFP-GG with IgE-FcϵRI, GD_{1b}, and Thy-1 were calculated and averaged over multiple sets of paired images. Co-redistribution was parameterized according to two characteristic features of the correlation curve: 1) peak height (ρ_o; Eq 4 with $j = 0$), which corresponds to the degree of correlation when the matched image profiles are perfectly aligned, and 2) peak area (*A*; Eq 5), which corresponds to both height and width of the average correlated aggregate peak that is assessed by systematically shifting one image profile with respect to the other. Because each of the curves in Fig. 6 represents an average of 6–24 individual curves, off-center peaks observed in individual correlations cancel out, as was shown with the simulations (Fig. 4 *b*). The averaged parameters ρ_o and *A* for image pairs from each type of sample are summarized in Figs. 8 and 9, respectively.

Figs. 6, 8, and 9 quantitatively confirm significant differences between the co-redistribution properties of PM-EGFP and EGFP-GG. With PM-EGFP (Fig. 6 *A*), cross-correlations with IgE-FcϵRI, GD_{1b}, and Thy-1 show strong heightening and broadening of the central peak after incubation at 4°C under cross-linking conditions. Co-redistribution with IgE-FcϵRI (Fig. 6 *A a*) differs from that with GD_{1b} and Thy-1 (Fig. 6 *A*, *b* and *c*, respectively) in two distinct ways: 1) the cross-correlation after initial incubation with the Cy3-labeled antibody (Table 1, condition 1) is much lower, both relative to the cross-linked IgE-FcϵRI case (Table 1, condition 2b) and in absolute magnitude compared with the GD_{1b} and Thy-1 samples under all three conditions, and 2) incubation at 4°C with no cross-linkers (Table 1, condition 2a) produces neither IgE-FcϵRI aggregates nor co-redistributed PM-EGFP. Thus, as shown previously with Lyn (Holowka et al., 2000) and as suggested by visualization (Fig. 5 *A*), PM-EGFP co-redistributes with cross-linked IgE-FcϵRI, GD_{1b}, and Thy-1 corresponding to their association with lipid rafts. GD_{1b} and Thy-1 evidently associate with rafts to some extent after the initial incubation with bivalent Cy3-anti-GD_{1b} and Cy3-anti-Thy-1, and this does not happen to the same extent with Cy3-IgE, which is monovalent for FcϵRI.

EGFP-GG samples compared with the same species under the same conditions exhibit cross-correlation curves that change significantly less after addition of secondary cross-linking agents at 4°C (Fig. 6 *B*). In particular, the EGFP-GG correlation with IgE-FcϵRI does not increase after the latter is cross-linked. As suggested by the visualized images (Fig. 5), this quantitative analysis confirms that co-redistribution with cross-linked species IgE-FcϵRI, GD_{1b}, and Thy-1 is less for EGFP-GG than for PM-EGFP (see Fig. 8, cross-hatched bars).

As another comparison to the EGFP constructs, we carried out cross-correlation analysis with Cdc42, a Rho-family GTPase that anchors to the inner leaflet by means of its geranylgeranyl chain (Ghomashchi et al., 1995) (Fig. 7).

FIGURE 5 Representative paired images of RBL cells expressing (*A*) PM-EGFP and (*B*) EGFP-CG. The cells are co-labeled with Cy3-modified primary antibodies: Cy3-IgE for FcϵRI (*column 1*), Cy3-AA4 for GD_{1b} (*column 2*), and Cy3-OX7 for Thy-1 (*column 3*). Images were taken either immediately after labeling (Table 1, condition 1) (*row 1*), after a 4–6 hr incubation at 4°C without (Table 1, condition 2a) (*row 2*), or with secondary crosslinking agents (Table 1, condition 2b) (*row 3*). Paired images represent the same cell viewed in different channels of the confocal microscope: *left*, EGFP fluorescence is visible; *right*, Cy3 fluorescence is visible. All cells were fixed, and fluorescence microscopy images were acquired as described in *Materials and Methods*. Cell diameters are ~10 μm.

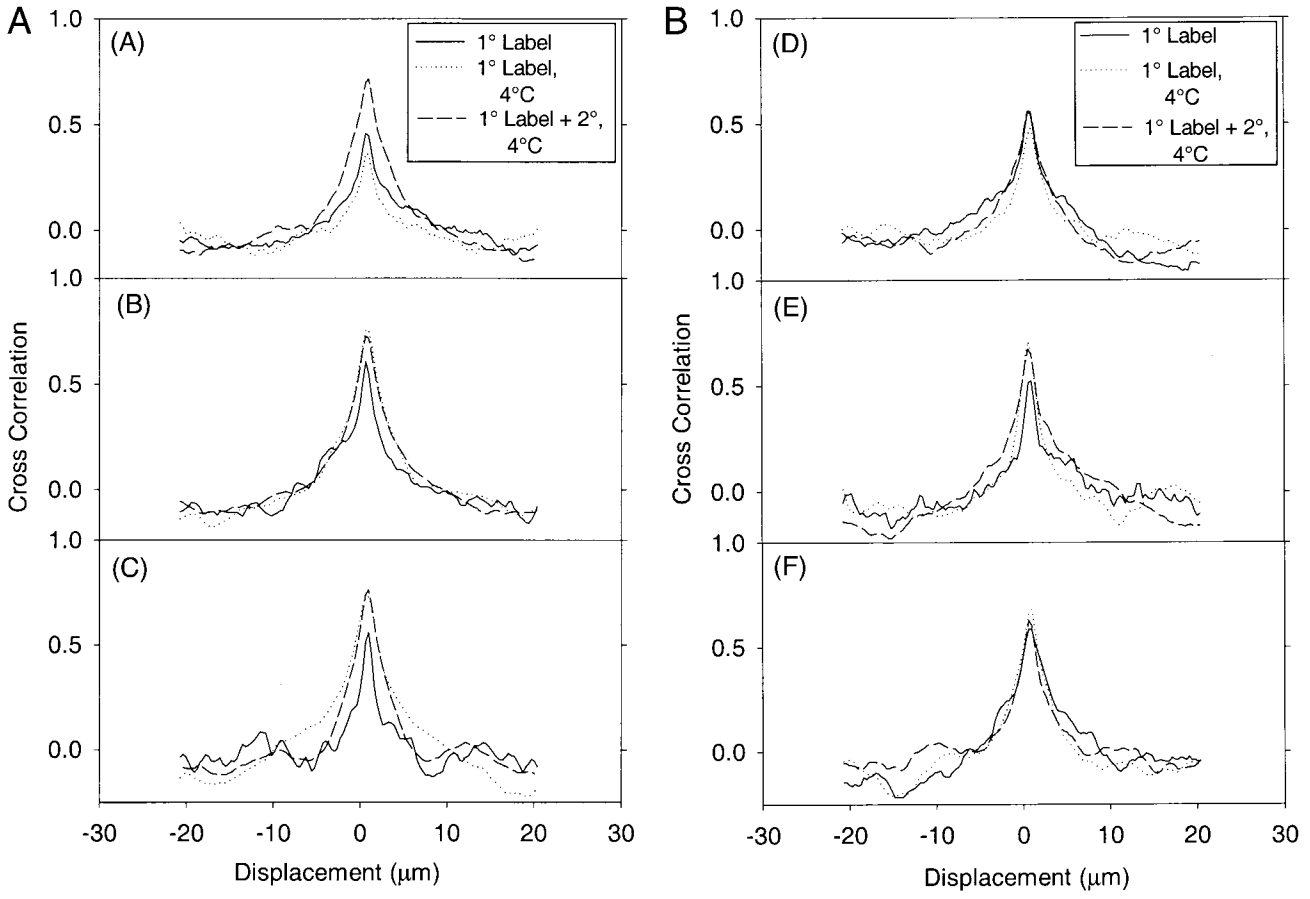

FIGURE 6 Cross-correlations of equatorial intensity profiles for cells expressing (*A*) PM-EGFP and (*B*) EGFP-GG. The EGFP fluorescence coupled to these constructs was correlated with Cy3 fluorescence coupled to: IgE-FcεRI (*a* and *d*); GD_{1b}; (*b* and *e*); and Thy-1 (*c* and *f*). For each set of dually labeled cells, three experimental conditions were investigated as described in Table 1: condition 1 (——), condition 2a (·····) and condition 2b (– – –). Each curve is an average of typically 15 (6 to 24) individual curves collected among several replicated experiments on different days. Included in these averages are data from the representative images in Fig. 5. Displacement is determined from the linear conversion between pixels and lateral distance known for the instrumental configuration of the confocal microscope.

With paired images similar to those in Fig. 5, we observed previously that Cdc42 does not co-redistribute with cross-linked IgE-FcεRI (Holowka et al., 2000). In a direct comparison (Figs. 6 and 7), there are notable differences among the cross-correlation curves of IgE-FcεRI with PM-EGFP, EGFP-GG, and Cdc42, after the 4- 6-h incubation at 4°C in the presence of secondary anti-IgE or multivalent antigen (Table 1, condition 2b). PM-EGFP clearly has the greatest propensity to co-redistribute; Cdc42 exhibits only a small positive cross-correlation with aggregated IgE-FcεRI; EGFP-GG is intermediate (Fig. 8, cross-hatched bars for IgE samples).

The *A* value, determined as the integrated area underneath a symmetric exponential fit to the correlation curve (Eq 5), serves as a useful parameter for co-redistributed aggregates and their relative sizes because it includes both peak height and width. We analyzed the data in Figs. 6 and 7 accordingly, as summarized in Fig. 9. Even more striking than with the ρ_o values, there is a clear trend to higher cross-correla-

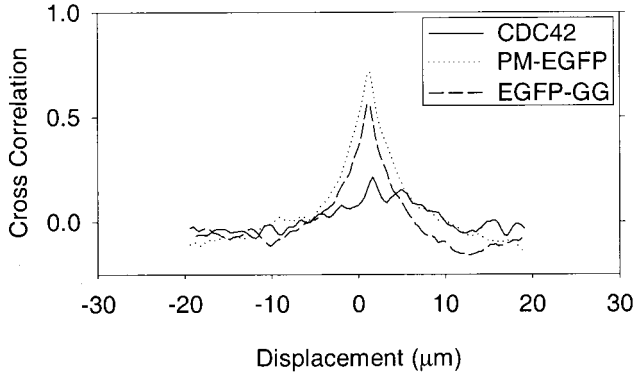

FIGURE 7 Cross-correlations of equatorial fluorescence intensity profiles comparing IgE-FcεRI with inner leaflet species PM-EGFP (·····), and EGFP-GG (– – –), Cdc42 (——), after a 4–6 hr incubation at 4°C with secondary cross-linking agents present (Table 1, condition 2b). Each curve is an average of typically 15 individual curves collected between several replicated experiments on different days. Displacement is determined as described in Fig. 6.

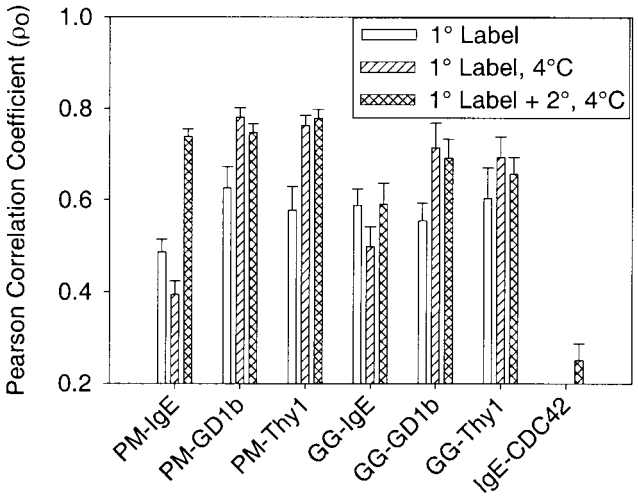

FIGURE 8 Summary of Pearson correlation coefficients ρ_o for averaged cross-correlation curves. Coefficients were calculated directly from the individual curves contributing to the averages using Eq. 4 with $j = 0$. The averaged ρ_o values correspond to the peaks of the averaged cross-correlation curves in Figs. 6 and 7. Error bars about the averages come from the individual curves and represent Student's t confidence limits (±68%).

tions for PM-EGFP from non-aggregating to aggregating conditions; there is no consistent trend with EGFP-GG. This is particularly distinct for the IgE samples (Fig. 9, compare open and cross-hatched bars). As expected from Fig. 7, the A value for cross-correlation of Cdc42 with cross-linked IgE-FcϵRI is comparatively very small.

DISCUSSION

This work resulted from our efforts to evaluate and quantify systematically co-localization of plasma membrane components in intact cells as observed with confocal microscopy. For this purpose we extended and refined previous applications of cross-correlation analysis (Stauffer and Meyer, 1997) by introducing normalization and developing expressions for two characteristic parameters, ρ_o and A. To aid interpretation, we generated a series of simulated cell profile traces designed to address particular issues. The focus of our specific application was an endogenous fluorescent analog for the tyrosine kinase Lyn (PM-EGFP), and we determined that the palmitate/myristylate modification of Lyn is sufficient for its membrane targeting and for its co-redistribution with cross-linked IgE-FcϵRI. For direct comparison with PM-EGFP, we constructed EGFP-GG, which anchors to the inner leaflet of the plasma membrane via a polyunsaturated geranylgeranyl chain and polybasic residues. Together with Cdc42, these inner leaflet membrane probes were evaluated for co-redistribution with transmembrane IgE-FcϵRI and also with outer leaflet components of lipid rafts, Thy-1 and ganglioside GD_{1b}.

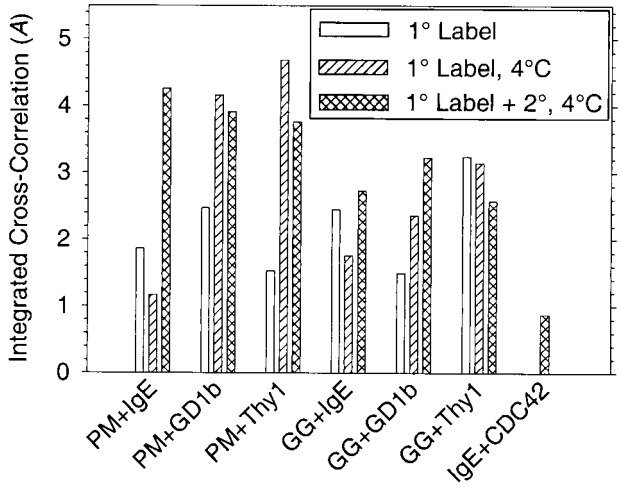

FIGURE 9 Summary of integrated areas under the averaged cross-correlation curves (A, Eq 5) represented in Figs. 6 and 7. There are no error bars because the A value is obtained directly from a single averaged curve in each case.

Simulated co-redistributions

Cross-correlation analysis (Eq. 4) provides a record of overlapping fluorescent intensities of dually labeled cells. The parameters ρ_o (Eq. 4, $j = 0$), which measures the extent of cross-correlating aggregates, and A (Eq. 5), which additionally measures the size of the aggregates, are particularly useful for direct comparisons. The numerical method we describe is generally applicable to equatorial (i.e., one-dimensional) traces of any shape. Image correlation spectroscopy is an alternate, two-dimensional method (Petersen et al., 1998) but requires relatively large, flat cell surface areas for useful analysis.

We considered a series of simulated equatorial traces (Fig. 1) that were based upon observed equatorial profiles of typical fluorescent species on the surface of RBL-2H3 cells with respect to aggregate sizes and relative intensities. Compared with a flat base, we find the rolling base more closely resembles the uniform distributions of species typically found in plasma membranes (Fig. 5). The normally distributed random noise that was added in incremental intensities to the simulated profiles (Fig. 1, c and d) is also representative of instrumental and systematic noise as observed in real confocal images. Cross-correlations of simulated traces serve as models for interpretation of data from dually labeled cells; the absolute height and width of the central peak characterize the correlative distributions of investigated species. Noise reduces absolute cross-correlation peak height (ρ_o), regardless of aggregate size (Figs. 2 and 3). The case of no aggregates serves as a model for uniformly distributed species on the cell surface (Fig. 2, a and b). Although the flat traces exhibit no cross-correlative peak, the rolling traces exhibit wide, strong peaks (Fig. 2 b). Thus, the morphology of cellular membranes alone can produce large absolute cross-correlation peaks. However, correlation

peaks due to morphology can be overpowered by noise (Fig. 2 *b*), allowing discrimination between this source and more intensely fluorescent aggregates. Another feature of cross-correlations is the off-center peaks, or tails that can arise for a single pair. They are due to random correlations at roughly xn ($n = 0, \pm1, \pm2, \ldots$) aggregate size intervals of alignment and may have little physical meaning. If random, these are eliminated when several curves are averaged (Fig. 4 *b*).

Mismatched traces illustrate other features of cross-correlation analyses. Although correlating membrane morphology with a small or large aggregate trace produces no central correlation peak, off-center peaks sometimes arise (Fig. 3, *b* and *c*). The same results are obtained when mismatched image profiles from two different real cells are cross-correlated as control samples (data not shown). Similar mismatches would be expected from cross-correlating profiles from a cell doubly labeled with a uniformly distributed species, together with an aggregated species, except that for a given cell both traces would share the same membrane morphology, which would heighten the central correlation peak. The mismatched large/small pair illustrates how the cross-correlation is diminished for traces with partially co-redistributed species (compare Fig. 3 *d* with Fig. 2, *c* and *d*). Table 2 provides useful values for theoretical limits for the cross-correlation parameter ρ_o compared with the range of values observed on cells in different cases. Although beyond the scope of the present study, this cross-correlation analysis could be further refined to distinguish between small and large aggregates on the same cell as would be reflected in the *A* parameter. This might allow one to determine, for example, whether there are cooperative effects on ρ_o for a given pair of probes. With the present analysis one can evaluate how a change in cross-correlation (ρ_o) compares with the corresponding change in average aggregate size (A), as illustrated below for IgE-FcεRI co-redistribution with PM-EGFP versus EGFP-GG.

Cross-correlations of distributions on RBL-2H3 cells

Analysis of PM-EGFP extended our previous observation that tyrosine kinase Lyn co-redistributes with aggregated IgE-FcεRI and other raft components in a functionally relevant manner (Sheets et al., 1999a; Holowka et al., 2000). PM-EGFP co-localizes preferentially with membrane regions surrounding aggregated IgE-FcεRI, whereas EGFP-GG co-localizes more weakly, and Cdc42 co-localizes minimally. This difference, related to lipid composition, is consistent with the hypothesis that specialized membrane domains or rafts with lipid properties that differ from the bulk of the cellular membrane are coalesced after FcεRI or other raft components are aggregated. Species that associate with such rafts tend to have saturated fatty acid chains, but they also could associate by other means. Because PM-EGFP contains only the N-terminal sequence of Lyn, and not the SH2, SH3, or catalytic domains of this protein (Resh, 1996), its selective co-localization with cross-linked FcεRI and raft components confirms the sufficiency of the acyl-chain-containing sequence to mediate these interactions. Previous efforts to map this interaction in a yeast two-hybrid assay found that a similar length (1–27) N-terminal sequence is not significantly different from an irrelevant control sequence in its capacity to bind FcεRI-β, although a longer sequence corresponding to the unique domain of the Lyn A (66 residues at the N-terminus) did show weak but statistically significant binding (Vonakis et al., 1997). These results underline the importance of lipid modification and the membrane context for the interactions we detect.

Before cross-linking, IgE-FcεRI appears uniformly distributed on the surface of cells, as do GD_{1b}, Thy-1, PM-EGFP, and EGFP-GG (Fig. 5, *top row*). During the initial incubation (Table 1, *condition* 1) Cy3-IgE binds monovalently to FcεRI whereas the Cy3-labeled antibodies specific for GD_{1b} and Thy-1 can bind bivalently. Long-term cold incubations (Table 1, condition 2a) clearly alter the distribution of GD_{1b} and Thy-1 from nearly uniform distributions to large (micrometer size) aggregates; this does not occur with IgE-FcεRI (Fig. 5, *middle row*). As expected, IgE-FcεRI changes from uniform to highly aggregated if a secondary cross-linking agent is present (Table 1, condition 2b; Fig. 5, *bottom row*). That GD_{1b} and Thy-1 do not appear any further aggregated by the secondary cross-linkers indicates either that these components exist as homo-oligomers in the plasma membrane and can be further clustered by the primary monoclonal antibodies AA4 and OX7 or that these bivalent antibodies cause coalescence of membrane domains that contain these components. The large surface areas occupied by these patches (Fig. 5, *middle* and *bottom rows*) support the latter explanation.

The ρ_o and A values provide reliable parameters for comparing cellular distributions. Variability of ρ_o over individual curves can be represented by error bars (Fig. 8). The A value comes from the averaged curves and contains both correlation and displacement information, thereby including information on average aggregate size (Fig. 9). With PM-EGFP, the trend to higher cross-correlation from non-aggregating to aggregating conditions is evident, particularly with IgE-FcεRI. In contrast, EGFP-GG shows little redistribution with cross-linked IgE-FcεRI. Overall, the EGFP-GG data show more variability than the PM-EGFP data. With GD_{1b} and Thy-1 under aggregating conditions, EGFP-GG exhibits slightly lower ρ_o values than does PM-EGFP in parallel samples (Fig. 8); furthermore, EGFP-GG has noticeably lower A values (Fig. 9). This suggests a weak propensity to interact with small aggregates of raft components and no enhanced tendency upon formation of large aggregates. The 20-amino-acid GG sequence contains eight basic residues that were included to ensure targeting of this

construct to the plasma membrane (Leventis and Silvius, 1998); these residues may increase the interaction of EGFP-GG with lipid rafts. In addition, the *trans* configuration of the unsaturated bases in the geranylgeranyl acyl chain (Yamane et al., 1991) make it more likely to partition into the liquid-ordered phase of the lipid rafts than a *cis*-unsaturated acyl chain.

Cdc42, like EGFP-GG, contains a geranylgeranyl chain that contributes to its anchoring to the inner leaflet of the plasma membrane, and it contains six basic residues at its C-terminus near this acyl chain. Cdc42 is uniformly distributed at the plasma membrane inner leaflet when IgE-FcϵRI is cross-linked (Holowka et al., 2000), as confirmed by cross-correlation analysis (Fig. 7) with correspondingly low values for ρ_o and A (Figs. 8 and 9, respectively). Given structural similarity at their C-termini, it is not yet clear why Cdc42 appears to partition less favorably into lipid rafts than EGFP-GG. Possibly, interactions of Cdc42 with other plasma membrane components affect this association.

The distinctive behavior of PM-EGFP as compared with EGFP-GG and Cdc42 is especially apparent with the A values, indicating that increasing recruitment of PM-EGFP with the aggregated raft components (IgE-FcϵRI, Thy-1, and GD_{1b}) accompanies increasing size of the corresponding specialized membrane areas. This difference rules out trapping of the EGFP probes as a simple explanation. These quantitative results are consistent with previous images of Lyn co-redistributions (Sheets et al., 1999a; Holowka et al., 2000) and support the hypothesis that aggregation of IgE-FcϵRI causes coalescence of lipid rafts that facilitate the productive interactions of FcϵRI with raft-associated Lyn, thereby initiating transmembrane signaling.

In summary, our comparative experiments demonstrate how cross-correlation analysis can be very useful for quantifying subjective visual evaluation and also for pointing to features that may not be obvious to the eye. Although we examined rounded RBL cells, a similar analysis may be performed on equatorial profiles of any cell size or shape that are readily obtainable by standard confocal fluorescence microscopy. Moreover, these experiments have established PM-EGFP and EGFP-GG as endogenous fluorescent probes of the plasma membrane inner leaflet with distinct properties, and they can be used to examine interactions and dynamics in intact cells. For example, we have extended our evaluation of fixed images with fluorescence photobleaching recovery and fluorescence correlation spectroscopy of living cells to measure differential lateral diffusion of these probes before and after cell activation mediated by aggregated IgE-FcϵRI (P. S. Pyenta, P. Schwille, W. W. Webb, D. Holowka, and B. Baird, manuscript in preparation).

We appreciate the guidance of Dr. Quibo Li in the preparation of the EGFP constructs.

This work was supported by grants from the National Institutes of Health, AI18306 and GM08267 (P.S.P.).

REFERENCES

Baird, B., E. D. Sheets, and D. Holowka. 1999. How does the plasma membrane participate in cellular signaling by receptors for immunoglobulin E? *Biophys. Chem.* 82:109–119.

Barlow, R. J. 1989. Statistics: A Guide to the Use of Statistical Methods in the Physical Sciences. John Wiley and Sons, Chichester, UK.

Brown, D. A., and E. London. 1997. Structure of detergent-resistant membrane domains: does phase separation occur in biological membranes? *Biochem. Biophys. Res. Commun.*240:1–7.

Brown, D. A., and E. London. 1998a. Functions of lipid rafts in biological membranes. *Annu. Rev. Cell Biol.* 14:111–136.

Brown, D. A., and E. London. 1998b. Structure and origin of ordered lipid domains in biological membranes. *J. Membr. Biol.* 164:103–114.

Field, K. A., D. Holowka, and B. Baird. 1995. FcϵRI-mediated recruitment of $p53/56^{lyn}$ to detergent-resistant membrane domains accompanies cellular signaling. *Proc. Natl. Acad. Sci., U.S.A.* 92:9201–9205.

Field, K. A., D. Holowka, and B. Baird. 1997. Compartmentalized activation of the high affinity IgE receptor within membrane domains. *J. Biol. Chem.* 272:4276–4280.

Fridriksson, E., P. Shipkova, E. Sheets, D. Holowka, B. Baird, and F. McLafferty. 1999. Quantitative analysis of phospholipids in functionally important membrane domains from RBL-2H3 mast cells using tandem high-resolution mass spectrometry. *Biochemistry.* 38:8056–8063.

Ge, M., K. A. Field, R. Aneja, D. Holowka, B. Baird, and J. Freed. 1999. ESR characterization of liquid ordered phase of detergent resistant membranes from RBL-2H3 cells. *Biophys. J.* 77:925–933.

Ghomashchi, F., X. Zhang, L. Liu, and M. H. Gelb. 1995. Binding of prenylated and polybasic peptides to membranes: affinities and intervesicle exchange. *Biochemistry.* 34:11910–11918.

Glomset, J. A., and C. C. Farnsworth. 1994. Role of protein modification reactions in programming interactions between ras-related GTPases and cell membranes. *Annu. Rev. Cell Biol.* 10:181–205.

Guo, N., G. R. Her, V. N. Reinhold, M. J. Brennan, and R. P. Siraganian. 1989. Monoclonal antibody AA4, which inhibits binding of IgE to high affinity receptors on rat basophilic leukemia cells, binds to novel α-galactosyl derivatives of ganglioside G_{D1b}. *J. Biol. Chem.* 264: 13267–13272.

Holowka, D., E. D. Sheets, and B. Baird. 2000. Interactions between FceRI and detergent-resistant membrane domains (rafts) are regulated by the actin cytoskeleton. *J. Cell Sci.* 113:1009–1019.

James, G. L., J. L. Goldstein, and M. S. Brown. 1995. Polylysine and CVIM sequences of K-rasB dictate specificity of prenylation and confer resistance to benzodiazepine peptidomimetic in vitro. *J. Biol. Chem.* 270:6221–6226.

James, P. W., S. C. Ley, A. I. Magee, and P. S. Kabouridis. 2000. The role of lipid rafts in T cell antigen receptor (TCR) signaling. *Semin. Immunol.* 12:23–34.

Kinet, J.-P. 1999. The high-affinity IgE receptor (FcϵRI): from physiology to pathology. *Annu. Rev. Immunol.* 17:931–972.

Leventis, R., and J. R. Silvius. 1998. Lipid-binding characteristics of the polybasic carboxy-terminal sequence of K-ras4B. *Biochemistry.* 37: 7640–7648.

Metzger, H. 1999. It's spring, and thoughts turn to allergies. *Cell.* 97: 287–290.

Montixi, C., C. Langlet, A. M. Bernard, J. Thimonier, C. Dubois, M. A. Wurbel, J. P. Chauvin, M. Pierres, and H. T. He. 1998. Engagement of T cell receptor triggers its recruitment to low-density detergent-insoluble membrane domains. *EMBO J.* 17:5334–5348.

Petersen, N. O., C. Brown, A. Kaminski, J. Rocheleau, M. Srivastava, and P. W. Wiseman. 1998. Analysis of membrane protein cluster densities and sizes in situ by image correlation spectroscopy. *Faraday Discuss.* 111:289–305.

Pierini, L., D. Holowka, and B. Baird. 1996. FcϵRI-mediated association of 6-μm beads with RBL-2H3 mast cells results in exclusion of signaling proteins from the forming phagosome and abrogation of normal downstream signaling. *J. Cell Biol.* 134:1427–1439.

Resh, M. D. 1996. Regulation of cellular signalling by fatty acid acylation and prenylation of signal transduction proteins. *Cell. Signal.* 8:403–412.

Rider, L. G., N. Raben, L. Miller, and C. Jelsema. 1994. The cDNAs encoding two forms of the LYN protein tyrosine kinase are expressed in rat mast cells and human myeloid cells. *Gene.* 138:219–222.

Schroeder, R. J., S. N. Ahmed, Y. Zhu, E. London, and D. A. Brown. 1998. Cholesterol and sphingolipid enhance the Triton X-100 insolubility of glycosylphosphatidylinositol-anchored proteins by promoting the formation of detergent-insoluble ordered membrane domains. *J. Biol. Chem.* 273:1150–1157.

Sheets, E. D., D. Holowka, and B. Baird. 1999a. Critical role for cholesterol in Lyn-mediated tyrosine phosphorylation of FcepsilonRI and their association with detergent-resistant membranes. *J. Cell Biol.* 145: 877–887.

Sheets, E. D., D. Holowka, and B. Baird. 1999b. Membrane organization in immunoglobulin E receptor signaling. *Curr. Opin. Chem. Biol.* 3:95–99.

Shenoy-Scaria, A. M., L. K. Gauen, J. Kwong, A. S. Shaw, and D. M. Lublin. 1993. Palmitylation of an amino-terminal cysteine motif of protein tyrosine kinases $p56^{lck}$ and $p59^{fyn}$ mediates interaction with glycosyl-phosphatidylinositol-anchored proteins. *Mol. Cell. Biol.* 13: 6385–6392.

Stauffer, T. P., and T. Meyer. 1997. Compartmentalized IgE receptor-mediated signal transduction in living cells. *J. Cell Biol.* 139:1447–1454.

Subramanian, K., D. Holowka, B. Baird, and B. Goldstein. 1996. The Fc segment of IgE influences the kinetics of dissociation of a symmetrical bivalent ligand from cyclic dimeric complexes. *Biochemistry.* 35: 5518–5527.

Tsien, R. Y. 1998. The green fluorescent protein. *Annu. Rev. Biochem.* 67:509–544.

van't Hof, W., and M. D. Resh. 1997. Rapid plasma membrane anchoring of newly synthesized $p59^{fyn}$: selective requirement for NH_2-terminal myristoylation and palmitoylation at cystein-3. *J. Cell Biol.* 136: 1023–1035.

Vonakis, B. M., H. Chen, H. Haleem-Smith, and H. Metzger. 1997. The unique domain as the site on Lyn kinase for its constitutive association with the high affinity receptor for IgE. *J. Biol. Chem.* 272:24072–24080.

Webb, Y., L. Hermida-Matsumoto, and M. D. Resh. 2000. Inhibition of protein palmitoylation, raft localization, and T cell signaling by 2-bromopalmitate and polyunsaturated fatty acids. *J. Biol. Chem.* 275: 261–270.

Xavier, R., and B. Seed. 1999. Membrane compartmentation and the response to antigen. *Curr. Opin. Immunol.* 11:265–269.

Yamane, H. K., C. C. Farnswarth, H. Xie, T. Evans, W. N. Howald, W. H. Gelb, J. A. Glomset, S. Clarke, and B. K.-K. Fung. 1991. Membrane-binding domain of the small G protein G25K contains an S-(all-*trans*-geranylgeranyl)cysteine methyl ester at its carboxyl terminus. *Proc. Natl. Acad. Sci. U.S.A.* 88:286–290.

Zhang, W., R. P. Trible, and L. E. Samelson. 1998. LAT palmitoylation: its essential role in membrane microdomain targeting and tyrosine phosphorylation during T cell activation. *Immunity.* 9:239–246.